Frontiers of Information Technology & Electronic Engineering
www.jzus.zju.edu.cn; engineering.cae.cn; www.springerlink.com
ISSN 2095-9184 (print); ISSN 2095-9230 (online)
E-mail: jzus@zju.edu.cn

# Joint radio frequency front-end and digital back-end antijamming scheme based on a metasurface antenna array*#

Yangming LOU†, Liang JIN†‡, Wenyu JIANG, Shuaifang XIAO

*PLA Strategic Support Force Information Engineering University, Zhengzhou 450000, China*

†E-mail: louyangming1991@outlook.com; liangjin@263.net

Received Feb. 26, 2023; Revision accepted June 8, 2023; Crosschecked Aug. 8, 2023

**Abstract:** An array's degree of freedom (DoF) determines the number of jamming incidents that can be managed and the antijamming performance. Conventional arrays can improve the DoF only by increasing the number of antennas. On the other hand, when the received signal is digitized, high-power jamming will reduce the number of bits used to represent the desired signal, further increasing the difficulty of back-end antijamming based on digital signal processing. In this paper, we propose a joint radio frequency (RF) front-end and digital back-end antijamming scheme based on a metasurface antenna array. The metasurface antennas can rapidly switch patterns when receiving signals, so that a single channel can be equivalent to multiple channels and increase the DoF. We use independent component analysis to estimate the channel and then optimize the array parameters under the minimum signal-to-jamming ratio constraint of each antenna. The proposed scheme works well under high-power jamming conditions by suppressing jamming at the RF front end and using a low-precision analog-to-digital converter. Simulation results show that the proposed scheme reduces the bit error rate of the received signals by one order of magnitude compared with the conventional array.

**Key words:** Antijamming; Multiple-input multiple-output; Metasurface antenna array; Independent component analysis

https://doi.org/10.1631/FITEE.2300113 **CLC number:** TN973.3

## 1 Introduction

With the broadcasting characteristics of electromagnetic waves, people can communicate freely without the limitations of cables, which brings great convenience to our life. However, with the rapid development of wireless communication technology, a large number of electromagnetic signals cause serious interference that cannot be ignored. Wireless communication interference can be divided into two categories: in-system and out-of-system.

The in-system interference comes mainly from different users in the same system with communication conflicts because the allocated communication resources are not orthogonal. For in-system users, prior information, such as signal format, frequency, and transmission order, can be used to design anti-interference schemes. Alternatively, it is possible to avoid interference by allocating independent resource blocks for different users according to communication protocols through multiple access techniques.

‡ Corresponding author

* Project supported by the National Natural Science Foundation of China (No. U22A2001) and the Program of Songshan Laboratory (included in the management of the Major Science and Technology Program of Henan Province), China (No. 221100211300-03)

# Electronic supplementary materials: the online version of this article (https://doi.org/10.1631/FITEE.2300113) contains supplementary materials, which are available to authorized users

ORCID: Yangming LOU, https://orcid.org/0000-0003-1673-2508; Liang JIN, https://orcid.org/0000-0001-6464-6263

In contrast, uncertainty exists for out-of-system interference, with a large part belonging to malicious attacks, which we usually call jamming. There are many types of malicious jamming attacks (Pirayesh and Zeng, 2022), and the constant jamming attack (Grover et al., 2014) is the most basic one, where the jammer sends high-powered, wide-band jamming over a long period. This type of jamming can significantly degrade communication performance without prior information, but it is inefficient. A channel-aware jamming attack (Cai et al., 2013), in which the jammer attacks only when it detects that legitimate users are communicating, is more flexible than constant jamming. In this attack, jamming can be sent to specific target users. In addition, jammers can send signal-like jamming (Gvozdenovic et al., 2020), which has a format similar to legitimate communication signals, and may contain pseudo-information with practical meaning. This jamming method further increases the difficulty of detecting and suppressing jamming for legitimate users.

Antijamming schemes have been widely studied to solve the problem of communication performance degradation caused by the above jamming attacks. The classic antijamming techniques are carried out mainly in the time-frequency domain. For example, channel-hopping techniques (Navda et al., 2007; Jeung et al., 2011) actively avoid jamming by detecting its presence in current working bands. The direct sequence spread spectrum technique (Harjula et al., 2011; Pinola et al., 2012), which spreads the signal spectrum with constant signal power, can effectively deal with narrowband jamming. With the development of multi-antenna technology, spatial antijamming techniques are becoming more and more popular. Spatial resources and time-frequency resources are independent. By allocating independent spatial communication resources, users in different locations will not interfere with each other, even if they share the same time-frequency resources. In other words, the receiver can resist jamming by taking advantage of the spatial differences.

One of the typical spatial antijamming methods is configuring different weights on each antenna to form beams that suppress jamming and enhance the desired signals according to the spatial channel. There are different weight-generation criteria for antijamming methods. The desired signals and the jamming incidents will be located in different subspaces if the array's degree of freedom (DoF) is sufficient. Therefore, we can project the received signals to the orthogonal space of the jamming subspace to eliminate the jamming (Yan et al., 2014, 2016), and the projection matrix consists of the received weights of the array. The array can adjust antenna weights to form beams according to the direction of signal arrival, aligning the null to the jamming while aligning the main lobe to the desired signal to improve the received signal-to-jamming ratio (SJR) (Sun et al., 2022). The spatial antijamming methods described above require prior information about the channel of the desired signal and the jamming or direction of arrival (DoA) estimation of all the signals. However, because jammers will not cooperate with legitimate users, estimating channels via reference sequences is challenging. DoA estimation based methods have good antijamming performance in scenarios where the signal has only a single or primary path, such as satellite communications. In multi-path scenarios, however, the performance of such schemes degrades due to the difficulty of forming a null to the jamming.

The blind source separation (BSS) based antijamming scheme can solve the above problems effectively. The main BSS technique is independent component analysis (ICA), which allows for recovering independent sources from a mixed signal without prior knowledge of the mixing matrix (Hyvärinen and Oja, 2000; Puntonet and Prieto, 2004). Because jammings and desired signals are usually independent, ICA has become a powerful tool for antijamming and can be widely used in many communication systems. In Huang et al. (2003) and Ghahramani et al. (2021), ICA was used in a radar system to suppress jamming and to improve tracking performance effectively. For satellite communication systems, Yang et al. (2019) analyzed the performance of an ICA-based antijamming scheme. Ge et al. (2018) used ICA to separate the jamming and solved the performance degradation problem due to high-power jamming in the main lobe during DoA estimation. Li et al. (2017) and Yang et al. (2018) used ICA in a full-duplex system for self-interference cancellation. The receiver used ICA to separate the interference directly without auxiliary receiving links.

ICA-based schemes can suppress jamming attacks when the channels are unknown, but some unresolved problems remain. For conventional antijamming methods, improving beam directivity

accuracy and null depth relies on increasing the DoF. Specifically, when the number of signals is unknown, the array can guarantee only the suppression of all jamming attacks by increasing the array's DoF as much as possible. For ICA-based antijamming methods, in most cases, effective source separation can be achieved only when the DoF exceeds the number of sources. Conventionally, people improve the DoF by adding antennas. However, this will lead to an increase in device size and power consumption, which is contrary to the miniaturization and portability development trend.

On the other hand, most spatial antijamming methods are implemented at the back end by digital signal processing. The accuracy of the back-end signals is determined by the number of analog-to-digital converter (ADC) quantization bits. We call the bits used to represent the desired signal the "effective bits." When high-power jamming attacks and the desired signals enter the radio frequency (RF) channel simultaneously, the receiver's automatic gain control (AGC) device will control the signal power to avoid exceeding the ADC range. However, attenuating all signals will significantly reduce the number of bits representing the desired signal because of the limited number of ADC bits. The information loss of desired signals occurs at the RF front end and is difficult to recover by back-end signal processing methods. It can seriously affect the performance of the back-end ICA, so RF front-end jamming suppression is needed.

Reconfigurable antennas use varactors (White and Rebeiz, 2009; Tawk et al., 2012), positive-intrinsic-negative (PIN) diodes (Nikolaou et al., 2006; Zhang et al., 2020), RF microelectromechanical system (RF-MEMS) switches (Chiao et al., 1999; Nikolaou et al., 2009; Grau et al., 2010), and other switching structures to change their electromagnetic characteristics and thus provide different responses to the same arriving signal. This allows reconfigurable antennas to process the signal at the RF front end and improves the array's DoF compared to conventional antennas. Wireless signals will suffer from multi-path effects during propagation, and the paths from the same source will reach the receiving antenna from different directions. Among several types of reconfigurable antennas, the pattern-reconfigurable antenna can change its response to signals from different directions, thus changing the way of path superposition.

As shown in Fig. 1, for narrowband signals, the paths cannot be distinguished by temporal differences, so the channel between Alice and Bob is a superposition of $L$ paths, and the complex gain of path $l$ is denoted by $\boldsymbol{\alpha}_l$. Bob is equipped with a pattern-reconfigurable antenna whose response at $\theta_l$ is $\boldsymbol{\phi}(\theta_l)$, so the composite channel between Alice and Bob can be expressed as

$$h=\sum_{l=1}^{L}\boldsymbol{\phi}(\theta_l)\boldsymbol{\alpha}_l=\boldsymbol{\phi}^{\mathrm{T}}\boldsymbol{\alpha}. \tag{1}$$

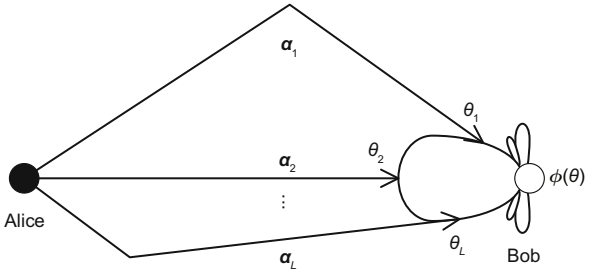


**Fig. 1 Paths superposed at the receiving antenna**

When Bob changes $\boldsymbol{\phi}$, the superposition of $\boldsymbol{\alpha}$ changes as well, which is equivalent to the signals experiencing different $h$. This shows that the pattern-reconfigurable antenna can use the DoF brought by multiple paths. Recently, the application of metamaterial technology in wireless communication has been widely studied. As shown in Fig. 2, the structure of the metasurface antenna is planar, consisting of massive compact spaced metamaterial elements. Each element can adjust the attenuation or phase of the incoming signals and can be treated as a phased array at the scale of a single antenna. Controlled by PINs or varactors, the metasurface can switch states within microseconds or even nanoseconds (Wu et al., 2021; Liang et al., 2022; Zhou et al., 2022).

While the metasurface antenna has a high DoF, its regular arrangement structure makes pattern design easier. Similar to conventional phased arrays, there is a Fourier transform between the element state and the pattern of the antenna:

$$h=\boldsymbol{\phi}^{\mathrm{T}}\boldsymbol{\alpha}=\boldsymbol{v}^{\mathrm{T}}\boldsymbol{A}\boldsymbol{\alpha}, \tag{2}$$

where $\boldsymbol{v}=[v_1,v_2,\ldots,v_I]^{\mathrm{T}}$ denotes the weights of the metamaterial elements, $I$ denotes the number of elements, and $\boldsymbol{A}$ is the manifold matrix, which

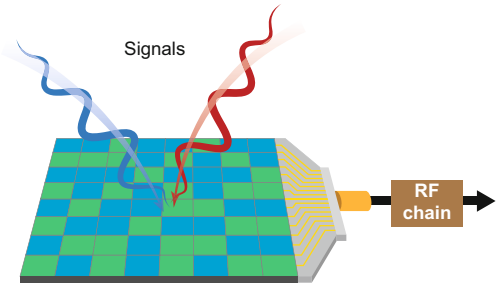


**Fig. 2 Structure of a metasurface antenna**

is determined by the arrangement of the elements. Therefore, the pattern-fitting problem is equivalent to the $\boldsymbol{v}$ design for the metasurface antenna. Moreover, using this high DoF to design the antenna, we can improve the front-end SJR, thus mitigating the ADC effective bit number degradation problem.

In this paper we propose an antijamming scheme based on the metasurface antenna array. The rapidly reconfigurable ability of the metasurface antenna is used to enhance the array's DoF. Then we use ICA to separate the signals with unknown jamming channels and optimally design the metasurface antenna parameters. The proposed scheme maximizes the received signal-to-jamming-plus-noise ratio (SJNR) of the array, while guaranteeing the single antenna SJR.

The contributions of the paper are summarized as follows:

1. We propose an array DoF improvement method based on metasurface antennas. We rapidly switch the patterns of the metasurface antennas during signal reception, so that one receiving channel of the antenna is equivalent to multiple channels. In this way, we can improve the array freedom by using the difference between paths. Also, randomly switching the antenna pattern can opportunistically suppress jamming and prevent the desired signal information from being completely lost due to the small number of ADC effective bits.

2. We propose a parameter design method for the metasurface antenna array to improve the number of ADC effective bits in high-power jamming conditions. We use ICA to blindly estimate the channel of the desired signals and the jammings, and then perform a joint design of the antenna parameters in the space-time domain. By adding a minimum SJR constraint at each antenna, we guarantee sufficient ADC effective bits and thus improve the performance of the antijamming algorithm based on back-end digital signal processing.

Notations used in this paper are as follows: A normal lowercase $a$ denotes a scalar, a bold lowercase $\boldsymbol{a}$ denotes a column vector, and a bold uppercase $\boldsymbol{A}$ denotes a matrix. The bold number $\mathbf{1}$ denotes a column vector with all entries of 1, while $\boldsymbol{I}$ and $\boldsymbol{O}$ denote the unit matrix and null matrix, respectively. $(\cdot)^*$, $(\cdot)^{\mathrm{T}}$, and $(\cdot)^{\mathrm{H}}$ denote the conjugate operation, transpose operation, and conjugate transpose operation, respectively. $|\cdot|$ denotes the absolute value. $\mathbb{E}[\cdot]$ denotes the expectation. $\mathrm{diag}(a, b, \cdots)$ denotes a diagonal matrix with $a, b, \cdots$ as diagonal entries, $\mathrm{diag}(\boldsymbol{A})$ denotes the column vector formed by the diagonal elements of $\boldsymbol{A}$, and $\mathrm{diag}(\boldsymbol{A}, \boldsymbol{B}, \dots)$ denotes the block diagonal array with $\boldsymbol{A}, \boldsymbol{B}, \dots$ as the diagonal. $\mathrm{tr}(\cdot)$ denotes the trace of the matrix, i.e., the sum of the elements on the diagonal.

## 2 System model

As shown in Fig. 3, the receiver, Alice, communicates with Bob using multiple transmitters. The transmitted signals are $\boldsymbol{x}_{\mathrm{S}} = [x_{\mathrm{S}1}, x_{\mathrm{S}2}, \cdots, x_{\mathrm{S}M_{\mathrm{S}}}]^{\mathrm{T}}$. Multiple jammers named Jammer send strong jamming signals, $\boldsymbol{x}_{\mathrm{J}} = [x_{\mathrm{J}1}, x_{\mathrm{J}2}, \cdots, x_{\mathrm{J}M_{\mathrm{J}}}]^{\mathrm{T}}$, on the same frequency to obstruct Alice's normal reception, where $M = M_{\mathrm{S}} + M_{\mathrm{J}}$. Both the transmitting signals and the jamming signals arrive at Alice via multiple paths.

Alice is equipped with an array of $N$ metasurface antennas. The received signal from antenna $n$ is shown in Eq. (3):

$$y_n = \sum_{m=1}^{M_{\mathrm{S}}} h_{nm}^{\mathrm{S}} x_{\mathrm{S}m} + \sum_{m=1}^{M_{\mathrm{J}}} h_{nm}^{\mathrm{J}} x_{\mathrm{J}m} + z_n. \quad (3)$$

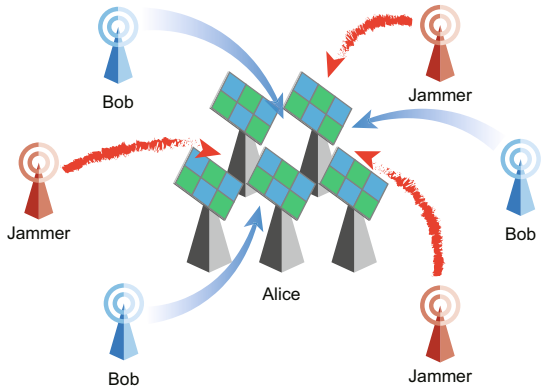


**Fig. 3 Multi-user multi-jamming scenario**
Alice is affected by Jammer's jamming when communicating with Bob

Considering Eq. (2), the channels of the desired signals and jamming signals can be expressed as $h_{nm}^{\mathrm{S}} = \boldsymbol{v}_n^{\mathrm{T}} \boldsymbol{A}_{nm}^{\mathrm{S}} \boldsymbol{\alpha}_m^{\mathrm{S}}$ and $h_{nm}^{\mathrm{J}} = \boldsymbol{v}_n^{\mathrm{T}} \boldsymbol{A}_{nm}^{\mathrm{J}} \boldsymbol{\alpha}_m^{\mathrm{J}}$, where $z_n$ is Gaussian white noise with power $\sigma^2$. We denote $\boldsymbol{S}_n \triangleq [\boldsymbol{A}_{n1}^{\mathrm{S}} \boldsymbol{\alpha}_1^{\mathrm{S}}, \boldsymbol{A}_{n2}^{\mathrm{S}} \boldsymbol{\alpha}_2^{\mathrm{S}}, \cdots, \boldsymbol{A}_{nM_{\mathrm{S}}}^{\mathrm{S}} \boldsymbol{\alpha}_{M_{\mathrm{S}}}^{\mathrm{S}}]$, $\boldsymbol{J}_n \triangleq [\boldsymbol{A}_{n1}^{\mathrm{J}} \boldsymbol{\alpha}_1^{\mathrm{J}}, \boldsymbol{A}_{n2}^{\mathrm{J}} \boldsymbol{\alpha}_2^{\mathrm{J}}, \cdots, \boldsymbol{A}_{nM_{\mathrm{J}}}^{\mathrm{J}} \boldsymbol{\alpha}_{M_{\mathrm{J}}}^{\mathrm{J}}]$. Then the above equation can be simplified to

$$y_n = \boldsymbol{v}_n^{\mathrm{T}} \boldsymbol{S}_n \boldsymbol{x}_{\mathrm{S}} + \boldsymbol{v}_n^{\mathrm{T}} \boldsymbol{J}_n \boldsymbol{x}_{\mathrm{J}} + z_n. \tag{4}$$

The received signals of the array can be expressed as

$$\boldsymbol{y} = \mathrm{diag}(\boldsymbol{v}_1^{\mathrm{T}}, \boldsymbol{v}_2^{\mathrm{T}}, \ldots, \boldsymbol{v}_N^{\mathrm{T}}) \begin{bmatrix} \boldsymbol{S}_1 & \boldsymbol{J}_1 \\ \boldsymbol{S}_2 & \boldsymbol{J}_2 \\ \vdots & \vdots \\ \boldsymbol{S}_N & \boldsymbol{J}_N \end{bmatrix} \begin{bmatrix} \boldsymbol{x}_{\mathrm{S}} \\ \boldsymbol{x}_{\mathrm{J}} \end{bmatrix} + \boldsymbol{z}. \tag{5}$$

We can optimally design $\boldsymbol{v}_n$ to achieve the maximum received SJNR if $\boldsymbol{S}_n$ and $\boldsymbol{J}_n$ are obtained. In the following discussion, we equalize the power of both the desired signal and the interference with the gain of the channel for convenience and generality. The entries in $\boldsymbol{x}_{\mathrm{S}}$ and $\boldsymbol{x}_{\mathrm{J}}$ are independent of each other and have a variance of 1.

## 3 Array DoF improvement based on the reconfigurable capability of a metasurface antenna

Starting with this section, we will explain how to use the metasurface antenna array to realize antijamming. The DoF of the array directly affects the antijamming performance. As for ICA, the dimension of the mixed signal usually needs to be higher than that of the sources to separate signals. In this way, improving the array's DoF becomes a critical issue.

In Eq. (5), we present the received signal model. $\boldsymbol{x}_{\mathrm{S}}$ and $\boldsymbol{x}_{\mathrm{J}}$ are projected into the received signal space as $[\boldsymbol{y}_1, \boldsymbol{y}_2, \cdots, \boldsymbol{y}_N]^{\mathrm{T}}$. To avoid losing the information after projection, the dimension of the projection space needs to be no smaller than that of the source space, i.e., $N \geq M = M_{\mathrm{S}} + M_{\mathrm{J}}$. The metasurface antenna can change $\boldsymbol{v}_n$, thus forming a new composite channel.

As shown in Fig. 4, the receiver rapidly switches $\boldsymbol{v}$ between sampling instants for receiving the same signal and divides the result according to $\boldsymbol{v}$ used at reception. For example, Alice uses the reconfigurable capability of the metasurface antenna to receive the signal at two different instants using $\boldsymbol{v}^{(1)}$ and $\boldsymbol{v}^{(2)}$, separately. As long as the divided signal satisfies the Nyquist theorem, the above processing is equivalent to the signal experiencing different channels. The joint processing of these signals increases the dimension of the received signal space.

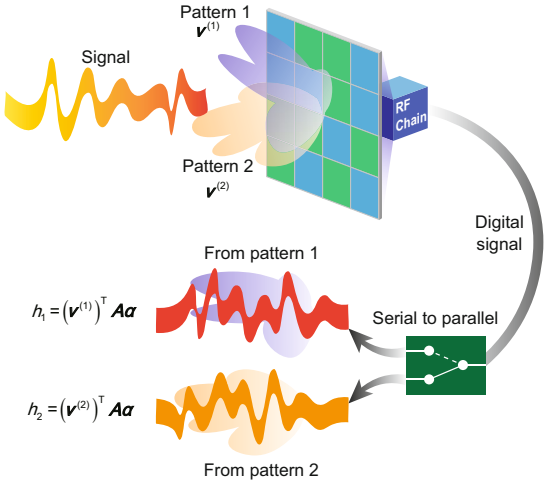


**Fig. 4 Signals and jamming signals received by rapidly switching antenna patterns**

If $\boldsymbol{v}_n^{(k)}$ denotes the parameters of the metasurface antenna $n$ at instant $k$ and $y_n^{(k)}$ denotes the received signal, then the signal model shown in Eq. (5) becomes

$$\begin{bmatrix} \boldsymbol{y}_1 \\ \boldsymbol{y}_2 \\ \vdots \\ \boldsymbol{y}_N \end{bmatrix} = \mathrm{diag}(\boldsymbol{V}_1^{\mathrm{T}}, \boldsymbol{V}_2^{\mathrm{T}}, \ldots, \boldsymbol{V}_N^{\mathrm{T}}) \begin{bmatrix} \boldsymbol{S}_1 & \boldsymbol{J}_1 \\ \boldsymbol{S}_2 & \boldsymbol{J}_2 \\ \vdots & \vdots \\ \boldsymbol{S}_N & \boldsymbol{J}_N \end{bmatrix} \begin{bmatrix} \boldsymbol{x}_{\mathrm{S}} \\ \boldsymbol{x}_{\mathrm{J}} \end{bmatrix} + \begin{bmatrix} \boldsymbol{z}_1 \\ \boldsymbol{z}_2 \\ \vdots \\ \boldsymbol{z}_N \end{bmatrix}, \tag{6}$$

where $\boldsymbol{V}_n = [\boldsymbol{v}_n^{(1)}, \boldsymbol{v}_n^{(2)}, \ldots, \boldsymbol{v}_n^{(K)}]$, $\boldsymbol{y}_n = [y_n^{(1)}, y_n^{(2)}, \ldots, y_n^{(K)}]^{\mathrm{T}}$, and the dimension of the received signal space where $y_n^{(k)}$ is located becomes $N \times K$. Therefore, by increasing the reconfiguration rate of the antenna, the DoF can be effectively increased compared with the conventional array. All columns of $\boldsymbol{V}_n$ should be of full rank to maximize the DoF. When $\boldsymbol{v}_n^{(1)} = \boldsymbol{v}_n^{(2)} = \cdots = \boldsymbol{v}_n^{(K)}$ and $\boldsymbol{V}_1 = \boldsymbol{V}_2 = \cdots = \boldsymbol{V}_N$, it means that the antennas in the array (i.e., the conventional antenna array)

are the same and will not change, which will make $y_n^{(1)} = y_n^{(2)} = \cdots = y_n^{(K)}$. The array's DoF decreases at this time. Therefore, the conventional antenna array can be regarded as a special form of the metasurface antenna array.

In addition to increasing the array's DoF, another problem to be addressed in this study is to mitigate the loss of reception performance caused by the degradation of the number of the effective ADC bits. The influence caused by this problem occurs at the RF front end and can be solved only by changing $\boldsymbol{V}_n$. Therefore, we can adopt an opportunistic jamming avoidance strategy with an unknown channel, i.e., randomly configuring $\boldsymbol{V}_n$. When $\boldsymbol{V}_n$ configured this time is not sufficient to cover the SJNR requirement for subsequent signal processing, a new set of parameters is re-switched for the reception to ensure that the following steps can proceed normally.

## 4 Optimized design of the metasurface antenna

### 4.1 Signal separation and channel estimation

Once the array receives signals through the randomly configured $\boldsymbol{V}_n$, we use ICA for further signal processing. For the signal model proposed in Eq. (6), the mixing matrix $\boldsymbol{H}$ for ICA is

$$\begin{aligned}\boldsymbol{H} &\triangleq \operatorname{diag}(\boldsymbol{V}_1^{\mathrm{T}}, \boldsymbol{V}_2^{\mathrm{T}}, \cdots, \boldsymbol{V}_N^{\mathrm{T}}) \begin{bmatrix} \boldsymbol{S}_1 & \boldsymbol{J}_1 \\ \boldsymbol{S}_2 & \boldsymbol{J}_2 \\ \vdots & \vdots \\ \boldsymbol{S}_N & \boldsymbol{J}_N \end{bmatrix} \\ &= \begin{bmatrix} \boldsymbol{V}_1^{\mathrm{T}}\boldsymbol{S}_1 & \boldsymbol{V}_1^{\mathrm{T}}\boldsymbol{J}_1 \\ \boldsymbol{V}_2^{\mathrm{T}}\boldsymbol{S}_2 & \boldsymbol{V}_2^{\mathrm{T}}\boldsymbol{J}_2 \\ \vdots & \vdots \\ \boldsymbol{V}_N^{\mathrm{T}}\boldsymbol{S}_N & \boldsymbol{V}_N^{\mathrm{T}}\boldsymbol{J}_N \end{bmatrix}. \end{aligned} \tag{7}$$

Our purpose is to find a separation matrix $\boldsymbol{B}$ that satisfies $\boldsymbol{B}^{\mathrm{H}}\boldsymbol{H} = \boldsymbol{I}$, to recover $\boldsymbol{x}_{\mathrm{S}}$ and $\boldsymbol{x}_{\mathrm{J}}$ from $\boldsymbol{y}_n$, that is,

$$\begin{bmatrix} \hat{\boldsymbol{x}}_{\mathrm{S}} \\ \hat{\boldsymbol{x}}_{\mathrm{J}} \end{bmatrix} = \boldsymbol{B}^{\mathrm{H}} \begin{bmatrix} \boldsymbol{y}_1 \\ \boldsymbol{y}_2 \\ \vdots \\ \boldsymbol{y}_N \end{bmatrix} = \begin{bmatrix} \boldsymbol{x}_{\mathrm{S}} \\ \boldsymbol{x}_{\mathrm{J}} \end{bmatrix} + \boldsymbol{B}^{\mathrm{H}} \begin{bmatrix} \boldsymbol{z}_1 \\ \boldsymbol{z}_2 \\ \vdots \\ \boldsymbol{z}_N \end{bmatrix}. \tag{8}$$

We obtain $\hat{\boldsymbol{H}}$, the estimate of the mixing matrix $\boldsymbol{H}$, and further complete the parameter configuration of all metasurface antennas based on $\hat{\boldsymbol{H}}$. The detailed steps for separating the signals and obtaining $\hat{\boldsymbol{H}}$ using ICA are shown in the supplementary materials. Here we summarize all steps in Algorithm 1.

**Algorithm 1** Iterative algorithm for CNM-ICA

1: Obtain the whitening matrix $\boldsymbol{F}$ according to Eq. (S4) and complete the whitening pre-processing
2: Initialize the separation matrix $\boldsymbol{W} = \boldsymbol{I}$, the number of iterations $i = 1$, and the difference threshold $\epsilon$
3: **repeat**
4: Update each column of $\boldsymbol{W}$ using Eq. (S11)
5: Orthogonalize $\boldsymbol{W}$ using Eq. (S12)
6: $i = i + 1$
7: **until** the difference between $\boldsymbol{W}(i+1)$ and $\boldsymbol{W}(i)$ is less than $\epsilon$, or the maximum number of iterations is reached

Note that the independent components separated by ICA have order and phase ambiguities. So, there are differences in the phase and order of the columns between $\hat{\boldsymbol{H}}$ and $\boldsymbol{H}$:

$$\boldsymbol{H} = \hat{\boldsymbol{H}}\boldsymbol{\Lambda}\boldsymbol{Q}, \tag{9}$$

where $\boldsymbol{\Lambda} = \operatorname{diag}(\mathrm{e}^{\mathrm{j}\theta_1}, \mathrm{e}^{\mathrm{j}\theta_2}, \cdots, \mathrm{e}^{\mathrm{j}\theta_M})$ represents the phase difference from the real channel, and $\boldsymbol{Q}$ is the permutation matrix. Therefore, $\hat{\boldsymbol{H}}$ needs to be preprocessed before the optimal design for $\boldsymbol{V}_n$. The ambiguity of the phase does not influence the antijamming problem we face in this study, but the ambiguity of the order will make it difficult to distinguish the desired signal channels from the jamming channels. The order ambiguity can be eliminated using part of the prior information of the desired signals. For example, we can do correlation analysis on the separated signals sequentially using the reference sequence of the desired signals. Those with high correlation peaks are the desired signals, while the rest are jamming signals. On the other hand, all jamming signals need to be suppressed, so there is no need to use the reference sequence for ordering. Therefore, we will ignore $\boldsymbol{\Lambda}$ and $\boldsymbol{Q}$ and let $\hat{\boldsymbol{H}} = \boldsymbol{H}$ in the following discussion.

We can use a sorting process to determine whether antijamming is effective at the front end. For example, suppose that the separated signals have no significant peaks when using the correlation peak based sorting method. In that case, we can believe that $\boldsymbol{V}_n$ configured is insufficient for following signal processing, so $\boldsymbol{V}_n$ needs to be regenerated for ICA.

### 4.2 Problem formulation

As described in the introduction, many existing studies use ICA for antijamming. However, when the ADC has a few effective bits, the low SJR at the antenna will lead to the failure of the signal separation, so $\boldsymbol{V}_n$ needs to be explicitly designed.

We need to adjust the parameters at each antenna so that the received signal that enters the RF channel has a sufficient SJR. In Section 2 we show that the signal power can equate to the channel, where all signals are independent and have a variance of 1. The natural channel can be written as follows:

$$\mathring{\boldsymbol{H}}=\begin{bmatrix}\boldsymbol{S}_1 & \boldsymbol{J}_1\\ \boldsymbol{S}_2 & \boldsymbol{J}_2\\ \vdots & \vdots\\ \boldsymbol{S}_N & \boldsymbol{J}_N\end{bmatrix}. \tag{10}$$

We define $\gamma$ as the minimum requirement for the SJR at antenna $n$, so we have

$$\mathrm{SJR}_n^{(m)}=\frac{\left(\boldsymbol{v}_n^{(m)}\right)^{\mathrm{T}}\boldsymbol{S}_n\boldsymbol{S}_n^{\mathrm{H}}\boldsymbol{v}_n^{(m)}}{\left(\boldsymbol{v}_n^{(m)}\right)^{\mathrm{T}}\boldsymbol{J}_n\boldsymbol{J}_n^{\mathrm{H}}\boldsymbol{v}_n^{(m)}}\geq\gamma. \tag{11}$$

However, Eq. (7) shows the form of the channel obtained by ICA, from which we cannot directly derive $\boldsymbol{S}_n$ and $\boldsymbol{J}_n$. Instead, it is possible to achieve

$$\hat{\boldsymbol{H}}=\mathrm{diag}(\check{\boldsymbol{V}}_1^{\mathrm{T}},\check{\boldsymbol{V}}_2^{\mathrm{T}},\cdots,\check{\boldsymbol{V}}_N^{\mathrm{T}})\mathring{\boldsymbol{H}}, \tag{12}$$

where $\check{\boldsymbol{V}}_n$ denotes the randomly initialized antenna parameters. Denote $\hat{\boldsymbol{H}}_{\boldsymbol{S}_n}=\check{\boldsymbol{V}}_n^{\mathrm{T}}\boldsymbol{S}_n$ and $\hat{\boldsymbol{H}}_{\boldsymbol{J}_n}=\check{\boldsymbol{V}}_n^{\mathrm{T}}\boldsymbol{J}_n$. We introduce the parameter update vector $\boldsymbol{u}_n^{(m)}$ as

$$\boldsymbol{v}_n^{(m)}=\check{\boldsymbol{V}}_n\left(\boldsymbol{u}_n^{(m)}\right)^*. \tag{13}$$

Then the SJR at antenna $n$ can be expressed as

$$\mathrm{SJR}_n^{(m)}=\frac{\left(\boldsymbol{u}_n^{(m)}\right)^{\mathrm{H}}\hat{\boldsymbol{H}}_{\boldsymbol{S}_n}\hat{\boldsymbol{H}}_{\boldsymbol{S}_n}^{\mathrm{H}}\boldsymbol{u}_n^{(m)}}{\left(\boldsymbol{u}_n^{(m)}\right)^{\mathrm{H}}\hat{\boldsymbol{H}}_{\boldsymbol{J}_n}\hat{\boldsymbol{H}}_{\boldsymbol{J}_n}^{\mathrm{H}}\boldsymbol{u}_n^{(m)}}\geq\gamma. \tag{14}$$

The conventional array can change only the weights of the received signals at the back end to form directional beams for antijamming, while the antennas at the front end are static. Using the reconfigurable capability of the metasurface antenna, we can reconfigure the antenna parameters for individual signals. The array receives $\boldsymbol{x}_m$ at instant $m$, aiming at the maximum SJNR. The remaining signals, denoted as $\boldsymbol{x}_{m'}$, are all jamming signals for $\boldsymbol{x}_m$. For convenience, we denote

$$\boldsymbol{v}_{(m)}^{\mathrm{T}}=\left[\left(\boldsymbol{v}_1^{(m)}\right)^{\mathrm{T}},\left(\boldsymbol{v}_2^{(m)}\right)^{\mathrm{T}},\cdots,\left(\boldsymbol{v}_N^{(m)}\right)^{\mathrm{T}}\right]^{\mathrm{T}}. \tag{15}$$

The natural channel experienced by $\boldsymbol{x}_m$ is the $m^{\mathrm{th}}$ column of $\mathring{\boldsymbol{H}}$, denoted as $\mathring{\boldsymbol{h}}_{(m)}$, and the remaining columns, denoted as $\mathring{\boldsymbol{H}}_{(m')}$, are the natural channels experienced by $\boldsymbol{x}_{m'}$. The array noise power is $N\sigma^2$, which is the sum of the noise power of each antenna, and the SJNR at instant $m$ is

$$\mathrm{SJNR}^{(m)}=\frac{\boldsymbol{v}_{(m)}^{\mathrm{T}}\mathring{\boldsymbol{h}}_{(m)}\mathring{\boldsymbol{h}}_{(m)}^{\mathrm{H}}\boldsymbol{v}_{(m)}^*}{\boldsymbol{v}_{(m)}^{\mathrm{T}}\mathring{\boldsymbol{H}}_{(m')}\mathring{\boldsymbol{H}}_{(m')}^{\mathrm{H}}\boldsymbol{v}_{(m)}^*+N\sigma^2}. \tag{16}$$

As with inequality (14), we define the update vector as

$$\boldsymbol{u}_{(m)}=\left[\left(\boldsymbol{u}_1^{(m)}\right)^{\mathrm{T}},\left(\boldsymbol{u}_2^{(m)}\right)^{\mathrm{T}},\ldots,\left(\boldsymbol{u}_N^{(m)}\right)^{\mathrm{T}}\right]^{\mathrm{T}}. \tag{17}$$

Then from Eq. (13) we have

$$\boldsymbol{v}_{(m)}=\begin{bmatrix}\check{\boldsymbol{V}}_1\left(\boldsymbol{u}_1^{(m)}\right)^*\\ \check{\boldsymbol{V}}_2\left(\boldsymbol{u}_2^{(m)}\right)^*\\ \vdots\\ \check{\boldsymbol{V}}_N\left(\boldsymbol{u}_N^{(m)}\right)^*\end{bmatrix}=\mathrm{diag}(\check{\boldsymbol{V}}_1,\check{\boldsymbol{V}}_2,\cdots,\check{\boldsymbol{V}}_N)\boldsymbol{u}_{(m)}^*. \tag{18}$$

We substitute Eq. (18) into Eq. (16). Then we have

$$\mathrm{SJNR}^{(m)}=\frac{\boldsymbol{u}_{(m)}^{\mathrm{H}}\hat{\boldsymbol{h}}_{(m)}\hat{\boldsymbol{h}}_{(m)}^{\mathrm{H}}\boldsymbol{u}_{(m)}}{\boldsymbol{u}_{(m)}^{\mathrm{H}}\hat{\boldsymbol{H}}_{(m')}\hat{\boldsymbol{H}}_{(m')}^{\mathrm{H}}\boldsymbol{u}_{(m)}+N\sigma^2}, \tag{19}$$

where $\hat{\boldsymbol{h}}_{(m)}$ denotes the channels corresponding to $\boldsymbol{x}_m$ in $\hat{\boldsymbol{H}}$, and $\hat{\boldsymbol{H}}_{(m')}$ denotes the remaining channels obviously:

$$\begin{cases}\hat{\boldsymbol{h}}_{(m)}=\mathrm{diag}(\check{\boldsymbol{V}}_1^{\mathrm{T}},\check{\boldsymbol{V}}_2^{\mathrm{T}},\cdots,\check{\boldsymbol{V}}_N^{\mathrm{T}})\mathring{\boldsymbol{h}}_{(m)},\\ \hat{\boldsymbol{H}}_{(m')}=\mathrm{diag}(\check{\boldsymbol{V}}_1^{\mathrm{T}},\check{\boldsymbol{V}}_2^{\mathrm{T}},\cdots,\check{\boldsymbol{V}}_N^{\mathrm{T}})\mathring{\boldsymbol{H}}_{(m')}.\end{cases} \tag{20}$$

In this way, after acquiring $\hat{\boldsymbol{H}}$, we first find $\boldsymbol{u}_{(m)}$ that maximizes Eq. (20) for the $m^{\mathrm{th}}$ signal, and then derive $\boldsymbol{v}_{(m)}$ from Eq. (18) to complete the array configuration. Because the metamaterial elements cannot enhance the power of the incident signals and can only attenuate the amplitude or shift the phase of

signals, the modulus of each element's weight should be $\leq 1$:

$$\left|\boldsymbol{v}_{(m)}\right|^2 \leq 1. \tag{21}$$

We can summarize the parameter design of the array as the following optimization problem:

$$\begin{aligned}\max_{\boldsymbol{u}_{(m)}}\ & \frac{\boldsymbol{u}_{(m)}^{\mathrm{H}}\hat{\boldsymbol{h}}_{(m)}\hat{\boldsymbol{h}}_{(m)}^{\mathrm{H}}\boldsymbol{u}_{(m)}}{\boldsymbol{u}_{(m)}^{\mathrm{H}}\hat{\boldsymbol{H}}_{(m')}\hat{\boldsymbol{H}}_{(m')}^{\mathrm{H}}\boldsymbol{u}_{(m)}+N\sigma^2}\\ \text{s.t.}\ & \frac{\left(\boldsymbol{u}_n^{(m)}\right)^{\mathrm{H}}\hat{\boldsymbol{H}}_{\boldsymbol{S}_n}\hat{\boldsymbol{H}}_{\boldsymbol{S}_n}^{\mathrm{H}}\boldsymbol{u}_n^{(m)}}{\left(\boldsymbol{u}_n^{(m)}\right)^{\mathrm{H}}\hat{\boldsymbol{H}}_{\boldsymbol{J}_n}\hat{\boldsymbol{H}}_{\boldsymbol{J}_n}^{\mathrm{H}}\boldsymbol{u}_n^{(m)}}\geq\gamma,\ n=1,2,\cdots,N,\\ & \left|\boldsymbol{v}_{(m)}\right|^2\leq 1.\end{aligned} \tag{22}$$

To further simplify the problem, we denote $\boldsymbol{u}_{(m)}$ and $\boldsymbol{u}_n^{(m)}$ as $\boldsymbol{u}$ and $\boldsymbol{u}_n$, respectively, and define

$$\begin{cases}\boldsymbol{R}=\hat{\boldsymbol{h}}_{(m)}\hat{\boldsymbol{h}}_{(m)}^{\mathrm{H}},\\ \boldsymbol{R}'=\hat{\boldsymbol{H}}_{(m')}\hat{\boldsymbol{H}}_{(m')}^{\mathrm{H}},\\ \boldsymbol{R}_{\boldsymbol{S}_n}=\mathrm{diag}(\boldsymbol{O},\hat{\boldsymbol{H}}_{\boldsymbol{S}_n}\hat{\boldsymbol{H}}_{\boldsymbol{S}_n}^{\mathrm{H}},\boldsymbol{O}),n=1,2,\cdots,N,\\ \boldsymbol{R}_{\boldsymbol{J}_n}=\mathrm{diag}(\boldsymbol{O},\hat{\boldsymbol{H}}_{\boldsymbol{J}_n}\hat{\boldsymbol{H}}_{\boldsymbol{J}_n}^{\mathrm{H}},\boldsymbol{O}),n=1,2,\cdots,N,\\ \check{\boldsymbol{V}}=\mathrm{diag}(\check{\boldsymbol{V}}_1,\check{\boldsymbol{V}}_2,\cdots,\check{\boldsymbol{V}}_N),\end{cases} \tag{23}$$

where $\boldsymbol{R}_{\boldsymbol{S}_n}$ and $\boldsymbol{R}_{\boldsymbol{J}_n}$ satisfy

$$\begin{cases}\boldsymbol{u}^{\mathrm{H}}\boldsymbol{R}_{\boldsymbol{S}_n}\boldsymbol{u}=\boldsymbol{u}_n^{\mathrm{H}}\hat{\boldsymbol{H}}_{\boldsymbol{S}_n}\hat{\boldsymbol{H}}_{\boldsymbol{S}_n}^{\mathrm{H}}\boldsymbol{u}_n,\\ \boldsymbol{u}^{\mathrm{H}}\boldsymbol{R}_{\boldsymbol{J}_n}\boldsymbol{u}=\boldsymbol{u}_n^{\mathrm{H}}\hat{\boldsymbol{H}}_{\boldsymbol{J}_n}\hat{\boldsymbol{H}}_{\boldsymbol{J}_n}^{\mathrm{H}}\boldsymbol{u}_n.\end{cases} \tag{24}$$

Then problem (22) can be rewritten as

$$\begin{aligned}\max_{\boldsymbol{u}}\ & \frac{\boldsymbol{u}^{\mathrm{H}}\boldsymbol{R}\boldsymbol{u}}{\boldsymbol{u}^{\mathrm{H}}\boldsymbol{R}'\boldsymbol{u}+N\sigma^2}\\ \text{s.t.}\ & \frac{\boldsymbol{u}^{\mathrm{H}}\boldsymbol{R}_{\boldsymbol{S}_n}\boldsymbol{u}}{\boldsymbol{u}^{\mathrm{H}}\boldsymbol{R}_{\boldsymbol{J}_n}\boldsymbol{u}}\geq\gamma,\ n=1,2,\cdots,N,\\ & \mathrm{diag}\left(\check{\boldsymbol{V}}^*\boldsymbol{u}\boldsymbol{u}^{\mathrm{H}}\check{\boldsymbol{V}}^{\mathrm{T}}\right)\leq 1.\end{aligned} \tag{25}$$

We can obtain the array configuration parameters at different instants by solving problem (25) for each signal, and the solution process is provided in the supplementary materials. Here we summarize all steps in Algorithm 2.

## 5 Simulation results

In this section, we demonstrate the performance of the proposed antijamming scheme based on the metasurface antenna array using simulations. Fig. 5 shows the array used at the receiver in our simulations.

**Algorithm 2** Optimization algorithm for metasurface antenna array antijamming

1: Randomly initialize the parameters of the metasurface antenna array $\check{\boldsymbol{V}}$ and receive the desired signals and jammings
2: Separate the desired signals from the jamming using Algorithm 1 and estimate the channel $\hat{\boldsymbol{H}}$
3: Perform the correlation analysis of the separated signals using the reference sequence of the desired signals
4: **if** clear correlation peaks appear and the desired signals can be distinguished from the jammings **then**
5: Go to line 9
6: **else**
7: Back to line 1
8: **end if**
9: Solve the optimization problem (25) for each signal to obtain the array antijamming parameters
10: Use the antijamming parameters to configure the array and received signals, and then separate the desired signals from the jammings using Algorithm 1 again

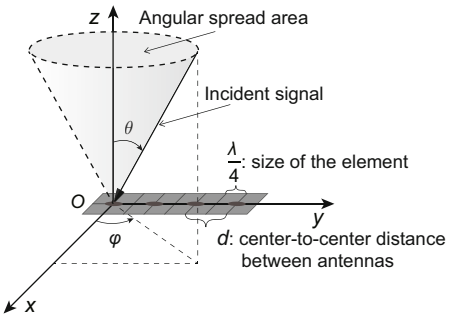


**Fig. 5 Structure of the metasurface antenna array for the simulations**
In our simulations, four metasurface antennas are uniformly arranged in the positive direction of the $y$-axis from the coordinate origin. Each antenna has four metamaterial elements centered at the antenna location, arranged in a $2\times2$ rectangle

### 5.1 Description of the simulation conditions

If not specified, the simulation parameters in this subsection are set as follows: the array consists of $N=4$ metasurface antennas, each consisting of $I=2\times2$ metamaterial elements. The number of parameter reconfigurations for each antenna is $K=4$, the element size is $\frac{\lambda}{4}$, and the antenna center-to-center distance is $d=\frac{\lambda}{2}$, where $\lambda$ denotes the wavelength. So, there is no space between two adjacent antennas. The incidence angles of the signal paths are in the cone-shaped area satisfying $\theta\in[0,\frac{\pi}{4}]$ and $\psi\in[0,2\pi]$. The number of paths $L$ for all signals

chosen randomly ranges from 2 to 6. The complex gain of paths obeys $\mathcal{CN}(0, \frac{1}{L})$. The channel can be calculated based on the model described in Eq. (2).

Two desired signals with power $P_{\mathrm{S}}$ and two jammings with power $P_{\mathrm{J}}$ are set up in the simulations. All signals are modulated with quadrature phase shift keying (QPSK) to emulate the influences caused by the signal-like jamming signals. For an arbitrary signal $\boldsymbol{x}_m$ with power $P_m$, before $L$ paths are merged at antenna $n$, the power at a metamaterial element is

$$\mathbb{E}\left[\mathbf{1}^{\mathrm{T}}\boldsymbol{\alpha}_m\boldsymbol{x}_m\boldsymbol{x}_m^{\mathrm{H}}\boldsymbol{\alpha}_m^{\mathrm{H}}\mathbf{1}\right]=\mathbf{1}^{\mathrm{T}}\mathbb{E}\left[\boldsymbol{\alpha}_m P_m\boldsymbol{\alpha}_m^{\mathrm{H}}\right]\mathbf{1}=P_m. \tag{26}$$

Therefore, the received jamming-to-signal ratio (JSR) in the simulations can be expressed as $\mathrm{JSR}=P_{\mathrm{J}}/P_{\mathrm{S}}$, and the signal-to-noise ratio (SNR) is constant at 15 dB. Each signal is quantized using eight-bit ADC after entering the channel. The length of the input symbol sequence for the ICA algorithm is 300, and the nonlinear function used is

$$\begin{cases} G(y)=\cosh(y), \\ g(y)=\sinh(y), \\ g'(y)=\cosh(y). \end{cases} \tag{27}$$

The antijamming performances in three array configurations are compared in the simulations:

1. Metasurface antenna multiple-input multiple-output (MESA MIMO) array. Each metasurface antenna has the same configuration parameters (i.e., $\boldsymbol{V}_1=\boldsymbol{V}_2=\cdots=\boldsymbol{V}_N$), each entry has an amplitude of 1, and the phase is chosen randomly in the range $[0, 2\pi)$. This condition is used to emulate the unknown channel case.

2. The $\gamma$-constrained optimized MESA MIMO ($\gamma$-MESA MIMO) array, which is the antijamming scheme proposed in this study. Based on MESA MIMO, the channel $\hat{\boldsymbol{H}}$ is obtained by ICA. The antenna parameters are optimized when the minimum SJR of the received signals (i.e., $\gamma$) is determined. When $\gamma=1$, $\gamma$-MESA MIMO is equivalent to MESA MIMO.

3. Conventional MIMO array. The model described in Eq. (6) is used in this condition, but all entries of $\boldsymbol{V}_n$ are 1, which means that each antenna in the array remains unchanged. We use this array configuration to emulate the conventional antenna structure.

Two performance criteria are used for evaluating the proposed scheme in the simulations. The first is the recognition rate (RR) of the desired signals. In this study, to ensure that the ADC has enough effective bits when there is no information about the channel, it is necessary to randomly configure the parameters of the metasurface antenna to mitigate the jamming signals. Then the desired signals are separated from the jamming signals by ICA. However, the ICA performance will degrade when the configured antenna parameters do not work well for jamming suppression. It may cause difficulty in distinguishing the reference sequence, which means that the recognition fails, and we need to generate a new $\boldsymbol{V}_n$ and repeat the above steps. We assume that the reference sequences of the desired signals have been known and can be distinguished by correlation analysis, whereby the RR is calculated. For MESA MIMO, we independently generate $\boldsymbol{V}_n$ each time and denote the RR as $P_{\mathrm{RR}}$. If $X$ denotes the number of repetitions before the recognition succeeds, then $X$ should obey the geometric distribution:

$$P(X=k)=(1-P_{\mathrm{RR}})^{k-1}P_{\mathrm{RR}}. \tag{28}$$

Then the probability of $X\le K$ is

$$\delta_K(P_{\mathrm{RR}})=P(X\le K)=\sum_{k=1}^{K}(1-P_{\mathrm{RR}})^{k-1}P_{\mathrm{RR}}. \tag{29}$$

For a given $K$, the larger the $\delta_K(P_{\mathrm{RR}})$ value, the more reliable the system. In the following simulations, we set $\delta_K(P_{\mathrm{RR}})\ge 0.9$ as the criterion for system reliability. In other words, the probability that there are fewer than three successful reconfigurations is $\ge 90\%$. According to Eq. (29), the minimum RR that guarantees the reliability of the system can be calculated to be about 0.54. We define this value as the reliability threshold. Another criterion is the bit error rate (BER) of the desired signals, and it is evident that under the same condition, a lower BER means a better antijamming performance.

The confidence level of the BER Monte Carlo simulations is related to the number of observation bits. When the confidence is $\ge 99\%$ and the accuracy is $10^{-k}$, the number of observation bits needed is about $10^{k+2}$ (Jeruchim, 1984). In communication, a BER $\le 10^{-3}$ is acceptable without additional coding, so the accuracy of BER estimation should be at least $10^{-4}$, and the number of samples needed is $10^6$.

According to the aforementioned conditions, the input symbol sequence for the ICA algorithm is 300 QPSK symbols, 600 bits in total, so it is necessary to obtain results by taking the average of 10 000 Monte Carlo simulations at each point.

### 5.2 Effects of JSR

Fig. 6 shows that the RR of the desired signals varies with the JSR. We can see that when the JSR is $\leq$ 35 dB, the RR of the desired signals is $\geq$ 0.95. However, after exceeding 40 dB, the RR drops rapidly and reaches the reliability threshold when the JSR is about 43 dB. Fig. 7 shows that the BER of the desired signals varies with the increasing JSR. For each of the configurations, the BER of the desired signals increases with the increasing JSR. MESA MIMO and $\gamma$-MESA MIMO are more effective at antijamming than conventional MIMO. At the high JSR, the suppression of jamming at the antenna can avoid decreasing the number of ADC effective bits. $\gamma$-MESA MIMO can reduce the BER by one order of magnitude, and a higher $\gamma$ can further improve the performance. However, in the low-bit JSR condition, jamming signals will not cause the number of effective bits to decrease. Due to the limited aperture of a single antenna, increasing $\gamma$ may also reduce signal power. Therefore, the loss caused by adding the constraint will exceed the antijamming gain. In this case, using smaller $\gamma$ or even MESA MIMO directly has a lower BER.

### 5.3 Effects of the number of ADC quantization bits

Another significant factor influencing the reception performance is the number of ADC quantization bits. As we can see in Fig. 8, the RR of the desired signals increases with the increasing number of quantization bits at a JSR of 40 dB and is always over the reliability threshold. When the number of quantization bits exceeds 10, the RR reaches almost 1.00. We can see from Fig. 9 that the BER of MESA MIMO starts to become lower than that of $\gamma$-MESA MIMO at this point, and different $\gamma$ values have almost the same effect on the BER. With a constant JSR, low-bit quantization will cause more losses on small signals (i.e., the desired signals). Thus, the reception performance can be effectively improved by suppressing the jamming signals at the front end. However,

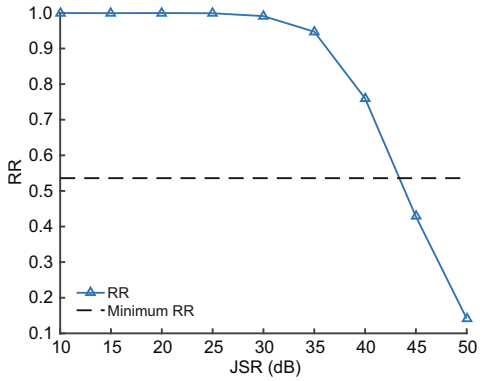


**Fig. 6 Recognition rate (RR) of the desired signals vs. the jamming-to-signal ratio (JSR)**

This indicates that the system is more stable with a JSR below 40 dB

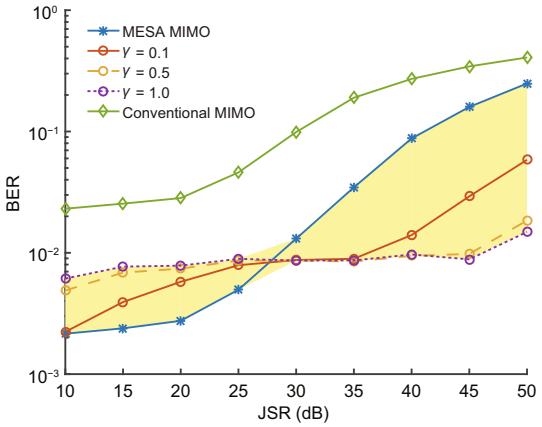


**Fig. 7 Bit error rate (BER) of the desired signals vs. the jamming-to-signal ratio (JSR)**

For each of the configurations, the BER of the desired signals increases with the increasing JSR. At a high JSR, the suppression of jamming at the antenna can avoid decreasing the number of ADC effective bits

with high-bit quantization, the small signal can obtain enough bits, and increasing the $\gamma$ constraint may weaken the small signal energy and reduce the BER.

### 5.4 Effects of angular spread

The spatial antijamming system relies on channel difference to suppress the jamming signals. A smaller angular spread makes the path arrival angle of the desired signals closer to that of the jamming signals, reducing the spatial difference and leading to performance degradation. It is clear from Fig. 10 that the desired signal RR is above the reliability threshold when the angular spread is $> 30°$. Fig. 11 shows that the BER of the desired signals varies with the angular spread of incident signals with a JSR of

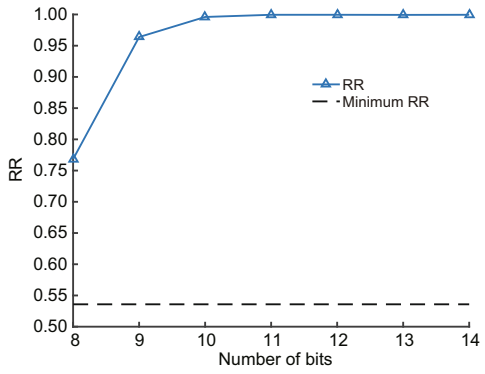


**Fig. 8 Recognition rate (RR) of the desired signals vs. the number of ADC quantization bits**

RR reaches almost 1.00 when the number of quantization bits exceeds 10

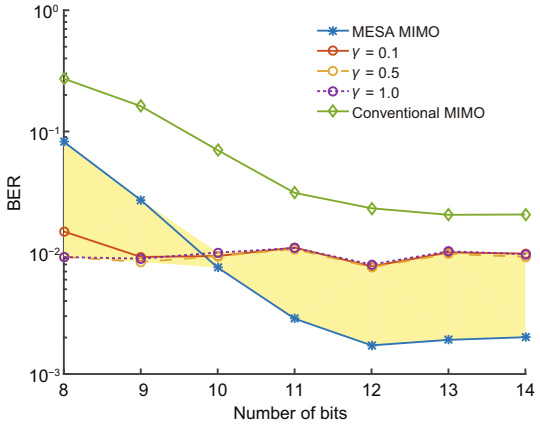


**Fig. 9 Bit error rate (BER) of the desired signals vs. the number of ADC quantization bits**

The antijamming performance can be effectively improved by suppressing the jamming signals at the front end when the number of ADC quantization bits is small

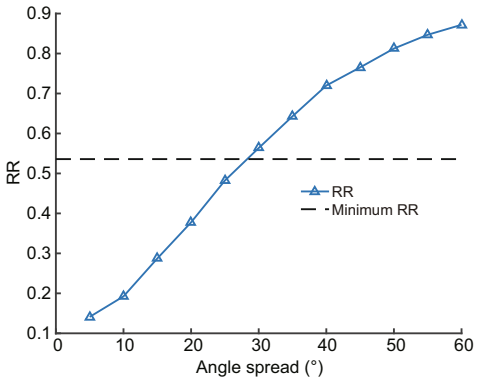


**Fig. 10 Recognition rate (RR) of the desired signals vs. the angular spread of incident signals**

RR of the desired signal is above the reliability threshold when the angular spread is $\geq 30°$

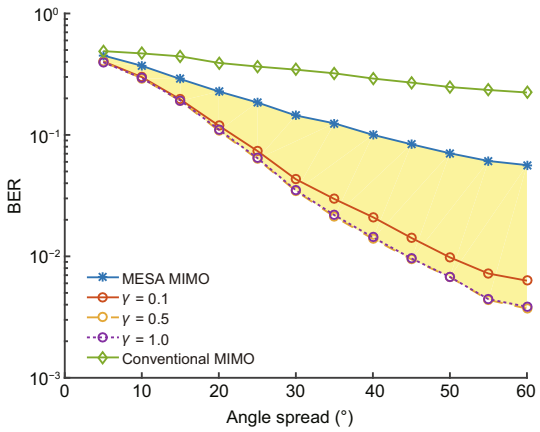


**Fig. 11 Bit error rate (BER) of the desired signals vs. the angular spread of incident signals**

The array has better antijamming performance with larger angular spreads when JSR is 40 dB and ADC is 8-bit

40 dB and 8-bit quantization. In this case, $\gamma$-MESA MIMO achieves the best antijamming performance. The small aperture of the antenna results in a limited angular resolution, which makes it challenging to produce a differential response to signals with different angles of arrival. Therefore, the array can achieve jamming suppression more easily with a larger angular spread. At an angular spread of 60°, the BER of $\gamma$-MESA MIMO can be reduced by two orders of magnitude compared to that of the conventional MIMO.

### 5.5 Effects of the number of paths

To present the effect of multiple paths more clearly, in this subsection, we no longer choose the number of paths randomly, but all signals have the same number of paths. In Eq. (6), we know that the conventional MIMO channel is the superposition of paths, so it loses multi-path information. Instead, MESA MIMO and $\gamma$-MESA MIMO can efficiently use the DoF from multiple paths by generating $\boldsymbol{V}_n$. Figs. 12 and 13 show the system antijamming performance varying with the number of paths. It can be seen that MESA MIMO and $\gamma$-MESA MIMO have better antijamming performance than conventional MIMO. With the increasing number of paths, the BERs of conventional MIMO and MESA MIMO are almost constant and slightly decrease, respectively, while that of $\gamma$-MESA MIMO decreases more significantly. The reason is that the difference between the paths of the desired signals and jamming signals increases as the number of paths grows. This spatial difference is beneficial for jamming suppression at the antenna. Therefore, for $\gamma$-MESA MIMO, the antijamming performance based on the channel

difference is much more easily influenced by the number of paths than that of the opportunistic jamming avoidance strategy adopted by MESA MIMO.

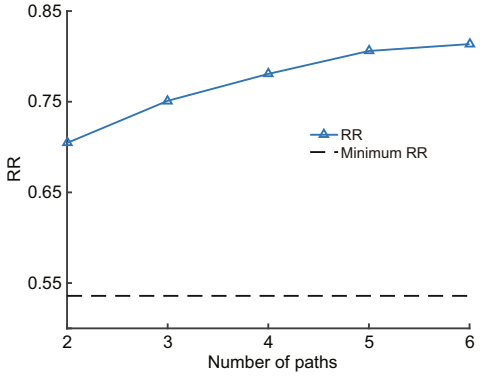


**Fig. 12 Recognition rate (RR) of the desired signals vs. the number of paths**

RR increases with the increase of the number of paths

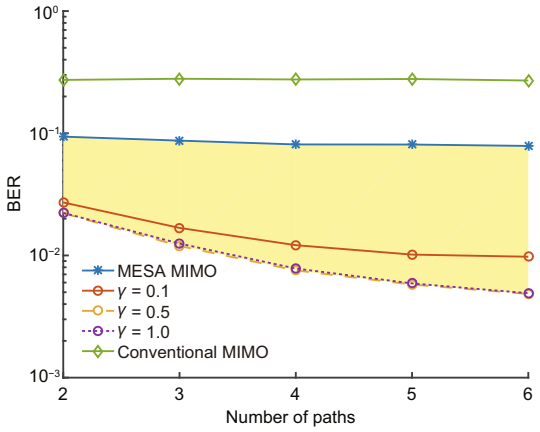


**Fig. 13 Bit error rate (BER) of the desired signals vs. the number of paths**

BER of $\gamma$-MESA MIMO decreases significantly

## 6 Conclusions

In this paper, we proposed a joint antijamming scheme based on a metasurface antenna array. We used the rapidly reconfigurable capability of the metasurface antenna to solve the problem of insufficient DoF. The metasurface antenna switched the configuration parameters rapidly, equivalent to creating multiple reception channels, thus increasing the array's DoF. The fast switching of antenna parameters allowed the RF front end to opportunistically avoid decrease of the number of ADC effective bits. Then we proposed a parameter optimization method for the metasurface antenna array. It used the blind channel estimation results obtained from ICA and can improve the number of ADC effective bits under high-power jamming. Simulation results showed that the proposed scheme could effectively improve the antijamming performance compared with conventional arrays and reduce the BER of the received signals by one order of magnitude.

## Contributors

Yangming LOU and Liang JIN designed the research. Yangming LOU and Wenyu JIANG processed the data. Yangming LOU drafted the paper. Liang JIN helped organize the paper. Liang JIN and Shuaifang XIAO revised and finalized the paper.

## Compliance with ethics guidelines

Yangming LOU, Liang JIN, Wenyu JIANG, and Shuaifang XIAO declare that they have no conflict of interest.

## Data availability

The data that support the findings of this study are available from the first or corresponding author upon reasonable request.

## References

Cai YF, Pelechrinis K, Wang X, et al., 2013. Joint reactive jammer detection and localization in an enterprise WiFi network. *Comput Netw*, 57(18):3799-3811. https://doi.org/10.1016/j.comnet.2013.09.004

Chiao JC, Fu Y, Chio IM, et al., 1999. MEMS reconfigurable Vee antenna. Proc IEEE MTT-S Int Microwave Symp Digest, p.1515-1518. https://doi.org/10.1109/MWSYM.1999.780242

Ge MM, Cui GL, Yu XX, et al., 2018. Mainlobe jamming suppression via blind source separation. Proc IEEE Radar Conf, p.914-918. https://doi.org/10.1109/RADAR.2018.8378682

Ghahramani H, Parhizgar N, Abbasi Arand B, et al., 2021. Convolutive complex-valued independent component analysis for nonlinear radar signal processing and maritime weak target detection. *Math Probl Eng*, 2021:6191303. https://doi.org/10.1155/2021/6191303

Grau A, Romeu J, Lee MJ, et al., 2010. A dual-linearly-polarized MEMS-reconfigurable antenna for narrowband MIMO communication systems. *IEEE Trans Antenn Propag*, 58(1):4-17. https://doi.org/10.1109/TAP.2009.2036197

Grover K, Lim A, Yang Q, 2014. Jamming and anti-jamming techniques in wireless networks: a survey. *Int J Ad Hoc Ubiq Comput*, 17(4):197-215. https://doi.org/10.1504/IJAHUC.2014.066419

Gvozdenovic S, Becker JK, Mikulskis J, et al., 2020. Truncate after preamble: PHY-based starvation attacks on IoT networks. 13th ACM Conf on Security and Privacy in Wireless and Mobile Networks, p.89-98. https://doi.org/10.1145/3395351.3399356

Harjula I, Pinola J, Prokkola J, 2011. Performance of IEEE 802.11 based WLAN devices under various jamming signals. MILCOM Military Communications Conf, p.2129-2135. https://doi.org/10.1109/MILCOM.2011.6127635

Huang GM, Yang LX, Su GQ, 2003. Blind source separation used for radar anti-jamming. Proc Int Conf on Neural Networks and Signal Processing, p.1382-1385. https://doi.org/10.1109/ICNNSP.2003.1281130

Hyvärinen A, Oja E, 2000. Independent component analysis: algorithms and applications. *Neur Netw*, 13(4-5):411-430. https://doi.org/10.1016/S0893-6080(00)00026-5

Jeruchim M, 1984. Techniques for estimating the bit error rate in the simulation of digital communication systems. *IEEE J Sel Areas Commun*, 2(1):153-170. https://doi.org/10.1109/JSAC.1984.1146031

Jeung J, Jeong S, Lim J, 2011. Adaptive rapid channel-hopping scheme mitigating smart jammer attacks in secure WLAN. MILCOM Military Communications Conf, p.1231-1236. https://doi.org/10.1109/MILCOM.2011.6127469

Li J, Zhang H, Fan ML, 2017. Digital self-interference cancellation based on independent component analysis for co-time co-frequency full-duplex communication systems. *IEEE Access*, 5:10222-10231. https://doi.org/10.1109/ACCESS.2017.2712614

Liang JC, Cheng Q, Gao Y, et al., 2022. An angle-insensitive 3-bit reconfigurable intelligent surface. *IEEE Trans Antenn Propag*, 70(10):8798-8808. https://doi.org/10.1109/TAP.2021.3130108

Navda V, Bohra A, Ganguly S, et al., 2007. Using channel hopping to increase 802.11 resilience to jamming attacks. 26th IEEE Int Conf on Computer Communications, p.2526-2530. https://doi.org/10.1109/INFCOM.2007.314

Nikolaou S, Bairavasubramanian R, Lugo C, et al., 2006. Pattern and frequency reconfigurable annular slot antenna using PIN diodes. *IEEE Trans Antenn Propag*, 54(2):439-448. https://doi.org/10.1109/TAP.2005.863398

Nikolaou S, Kingsley ND, Ponchak GE, et al., 2009. UWB elliptical monopoles with a reconfigurable band notch using MEMS switches actuated without bias lines. *IEEE Trans Antenn Propag*, 57(8):2242-2251. https://doi.org/10.1109/TAP.2009.2024450

Pinola J, Prokkola J, Piri E, 2012. An experimental study on jamming tolerance of 3G/WCDMA. IEEE Military Communications Conf, p.1-7. https://doi.org/10.1109/MILCOM.2012.6415651

Pirayesh H, Zeng HC, 2022. Jamming attacks and anti-jamming strategies in wireless networks: a comprehensive survey. *IEEE Commun Surv Tut*, 24(2):767-809. https://doi.org/10.1109/COMST.2022.3159185

Puntonet CG, Prieto A, 2004. Independent Component Analysis and Blind Signal Separation. Fifth Int Conf on Independent Component Analysis and Signal Separation, p.1-8. https://doi.org/10.1007/b100528

Sun YF, Chen FQ, Lu ZK, et al., 2022. Anti-jamming method and implementation for GNSS receiver based on array antenna rotation. *Remote Sens*, 14(19):4774. https://doi.org/10.3390/rs14194774

Tawk Y, Costantine J, Christodoulou CG, 2012. A varactor-based reconfigurable filtenna. *IEEE Antenn Wirel Propag Lett*, 11:716-719. https://doi.org/10.1109/LAWP.2012.2204850

White CR, Rebeiz GM, 2009. Single- and dual-polarized tunable slot-ring antennas. *IEEE Trans Antenn Propag*, 57(1):19-26. https://doi.org/10.1109/TAP.2008.2009664

Wu QQ, Zhang SW, Zheng BX, et al., 2021. Intelligent reflecting surface-aided wireless communications: a tutorial. *IEEE Trans Commun*, 69(5):3313-3351. https://doi.org/10.1109/TCOMM.2021.3051897

Yan QB, Zeng HC, Jiang TT, et al., 2014. MIMO-based jamming resilient communication in wireless networks. IEEE Conf on Computer Communications, p.2697-2706. https://doi.org/10.1109/INFOCOM.2014.6848218

Yan QB, Zeng HC, Jiang TT, et al., 2016. Jamming resilient communication using MIMO interference cancellation. *IEEE Trans Inform Forens Sec*, 11(7):1486-1499. https://doi.org/10.1109/TIFS.2016.2535906

Yang H, Zhang H, Zhang J, et al., 2018. Digital self-interference cancellation based on blind source separation and spectral efficiency analysis for the full-duplex communication systems. *IEEE Access*, 6:43946-43955. https://doi.org/10.1109/ACCESS.2018.2864112

Yang H, Zhang H, Zhang J, et al., 2019. Blind source separation for satellite communication anti-jamming. Proc 10th Int Conf on Wireless and Satellite Systems, p.717-726. https://doi.org/10.1007/978-3-030-19153-5_70

Zhang J, Zhang S, Ying ZN, et al., 2020. Radiation-pattern reconfigurable phased array with p-i-n diodes controlled for 5G mobile terminals. *IEEE Trans Microw Theory Tech*, 68(3):1103-1117. https://doi.org/10.1109/TMTT.2019.2949790

Zhou QY, Wu JW, Wang SR, et al., 2022. Two-dimensional direction-of-arrival estimation based on time-domain-coding digital metasurface. *Appl Phys Lett*, 121(18):181702. https://doi.org/10.1063/5.0124291

## List of supplementary materials

1 Blind signal separation and channel estimation based on ICA

2 Optimum solution to problem (25)